ChemPhysChem

Research Article
doi.org/10.1002/cphc.202400328

Chemistry Europe
European Chemical Societies Publishing

www.chemphyschem.org

Velocity Map Imaging Photoelectron Spectroscopy of Silver Iodide Aerosol Particles

Danijela Danilović,*[a] Laurent Nahon,[b] Gustavo A. Garcia,[b] Aleksandar R. Milosavljević,[b] Nenad Vukmirović,[c] Radovan Dojčilović,[a] Dragana Tošić,[a] Vladimir Djoković,[a] and Dušan K. Božanić*[a]

The valence band electronic structure of isolated silver iodide nanoparticles (AgI NP) was investigated by vacuum-ultraviolet aerosol photoelectron spectroscopy using the velocity map imaging technique (VUV VMI-PES). The VUV VMI-PES results were obtained for polydisperse aerosol produced by aggregation of hydrocolloid of silver iodide particles 8–15 nm in size. The ionization energy of the AgI particles was found to be 6.0 ± 0.1 eV with respect to the vacuum level. The DFT calculations showed that the main contribution to the density of AgI electronic states in the valence region originates from I 5p orbitals. The dependence of the asymmetry parameter on the electron energy showed that the value of the characteristic energy loss of excited photoelectrons was 2.7 eV, which coincided with the band gap of the nanomaterial.

Introduction

Silver iodide (AgI), a semiconductor with a direct band gap of around 2.8 eV,[1] is one of the most promising materials for solid-state ionic conductors that can be employed in electrochemical devices.[2] Silver iodide in cubic α-AgI form, which is stable at temperatures above 420 K,[3] is one of the most efficient solid-state superionic conductors.[4] A significant amount of the research effort has been directed towards stabilization of the superionic α phase at lower temperatures by either decreasing the size of crystals to nanometer dimensions,[5,6] or by increasing the pressure.[7] In a recent study, Yamamoto et al[8] combined both approaches simultaneously. Besides the ionic conductivity, AgI NPs were studied for application in photocatalysis,[9,10] or as antimicrobial agents against various pathogens.[11,12] It was shown that improved photocatalytic and antimicrobial properties of AgI NPs can be achieved by hybridization with other materials.[13,14] In addition, recent reports showed increased interest in AgI materials and their hybrids with bismuth and copper halides. The AgI-BiI_3 and AgI-CuI hybrid thin films proved to be promising materials for developing novel light absorbers for photovoltaic devices.[15–18] The aforementioned applications critically depend on the electron structure of AgI nanoparticles, as well as the alignment of its valence levels with the valence levels of other components in the systems under consideration.

In this context, we report on the valence band electronic structure of silver iodide (AgI) aerosol particles studied by synchrotron vacuum-ultraviolet radiation velocity map imaging aerosol photoelectron spectroscopy (VUV VMI-PES). Aerosol photoelectron spectroscopy (APS) is a photoemission spectroscopy technique that relies on the interaction of a focused beam of submicrometer particles isolated in high-vacuum conditions with vacuum ultraviolet (VUV)[19] or soft X-ray synchrotron radiation.[20] This technique accesses the electronic properties of isolated particles while avoiding the effects of interaction with substrate, radiation damage, or charge accumulation on the electronic structure.[21] A suitable technique for measuring the distribution of the photoemitted electrons from gas-phase species according to their kinetic energy and photoemission angle is velocity map imaging (VMI).[22] In the case of VUV aerosol photoemission, the electron images obtained by the VMI might be asymmetrical with respect to the direction of the propagation of incident radiation.[23,24] The asymmetry can be manifested either as "shadowing",[23] in which the photoemission from the directly irradiated particle side is more pronounced, or as "nanofocusing",[24] in which the induced electric field is focused on the far side of the particle, effectively amplifying photoemission in the direction of the propagation of the incident radiation. These effects are mainly due to the interplay between asymmetrical absorption of the incident radiation and the electron scattering processes within the particle. They can be used to discriminate between the electrons emitted from the nanoparticles and those emitted from the gas-phase molecules, as well as to assess different properties of aerosol material related to the photoexcitation and electron transport processes.

Different single-phased and hybrid nanomaterials have been analyzed by VUV VMI-PES so far to study different aspects

[a] Dr. D. Danilović, Dr. R. Dojčilović, Dr. D. Tošić, Dr. V. Djoković, Dr. D. K. Božanić
Center of Excellence for Photoconversion
Vinča Institute of Nuclear Sciences - National Institute of Republic of Serbia, University of Belgrade
P.O. Box 522, 11001 Belgrade, Serbia
E-mail: danijelad@vin.bg.ac.rs
bozanic@vin.bg.ac.rs

[b] Dr. L. Nahon, Dr. G. A. Garcia, Dr. A. R. Milosavljević
Synchrotron SOLEIL
St. Aubin, BP48, 91192 Gif sur Yvette Cedex, France

[c] Dr. N. Vukmirović
Institute of Physics Belgrade, University of Belgrade
Pregrevica118, 11080 Belgrade, Serbia

Supporting information for this article is available on the WWW under https://doi.org/10.1002/cphc.202400328

of photoemission from isolated nanoparticles.[20,23,25–30] For instance, Wilson and coworkers measured the inelastic mean free path of electrons in core-shell nanostructures by varying shell thickness,[25] Tigrine et al. reported on absolute ionization cross-sections of tholin aerosols[26] while Sussmann et al. investigated attosecond size-dependent near field dynamic in isolated silica particles.[27] In our previous studies, we used VUV VMI-PES to study angle-resolved photoemission in isolated Ag_2S[28] and Au[29] nanoparticles. We also showed that VUV VMI-PES can provide valuable information about interfacial charge transfer between TiO_2 nanoparticles and organic molecules[30] as well as about the influence of ligand molecules on the valence electronic structure of $CH_3NH_3PbBr_3$ perovskite nanoparticles.[20]

In this study, we report on the electron energy and angular distributions of the valence electrons emitted from isolated silver iodide nanoparticles after the interaction with VUV synchrotron radiation. Obtained photoemission data were discussed and interpreted with the results from density functional theory calculations.

Results and Discussion

Characterization of Silver Iodide Nanoparticles

The results of the characterization of AgI NPs, henceforth termed primary AgI particles, are presented in Figure 1. Morphology and the size distribution of the primary particles were examined by atomic force microscopy (AFM). A typical AFM image of the sample is shown in Figure 1a. It reveals that AgI particles have irregular spherical shapes and uniform size distribution. It can be noted that the lateral dimensions of the observed particles are smaller than 50 nm, i.e., their lateral dimensions are in the size range in which they can be significantly affected by the AFM tip used in the intermittent contact mode.[31] Therefore, in the AFM analysis, we considered the vertical dimensions of the particles only. The distribution of the particles' heights is given in Figure 1b. The sizes of primary particles follow a log-normal distribution curve with a mean value of 10 ± 2 nm. The UV–Vis absorption spectrum of AgI hydrocolloid is presented in Figure 1c. The spectrum exhibits an onset of absorption at approximately 2.9 eV, which is in accordance with the reported band gap values for AgI nanoparticles[32] of dimensions larger than the exciton Bohr radius of the material.

VUV VMI-PES of Isolated AgI Nanoparticles

The VUV VMI-PES experiments were performed on a focused beam of aerosol particles produced by atomization of the primary AgI hydrocolloids, as described in the Methods section. The SMPS analyses (Supporting information, Figure S1) showed that the particle beam is comprised of polydisperse AgI aerosol particles, with the size distribution centered at approximately 100 nm. Each aerosol particle consists of an aggregate of individual primary AgI particles.

The background-corrected photoelectron image for AgI aerosols obtained at 11 eV photon energy is presented in Figure 2a. The image represents the distribution of the momenta (velocities) of the photoemitted electrons projected onto the plane of a two-dimensional position-sensitive detector. Regardless of their point of origin, the photoelectrons with the same velocity are projected on the same position of the image, with radial and polar coordinates of each position corresponding to the intensity and orientation of the velocity vector, respectively. In the case of AgI aerosols, the image shows clear asymmetry along the direction of the propagation of VUV radiation (represented by vertical arrows in Figures 2a and 2b). This effect, which was initially recognized by Wilson et al.[23] and subsequently analyzed in different studies,[29,33,34] is a consequence of the electron scattering and the attenuation of the VUV photon beam in aerosol particles. More specifically, since the values of electron scattering lengths (few nm) are smaller in comparison to the photon attenuation depths (few tens of nm), an excess of the photoelectrons is being emitted on the irradiated side.

This forward/backward asymmetry in the electron images leads to limitations of the symmetry conditions required for the reconstruction of the three-dimensional distribution of photoelectron momenta and, consequently, proper assessment of the photoelectron spectra. These restrictions can be circumvented

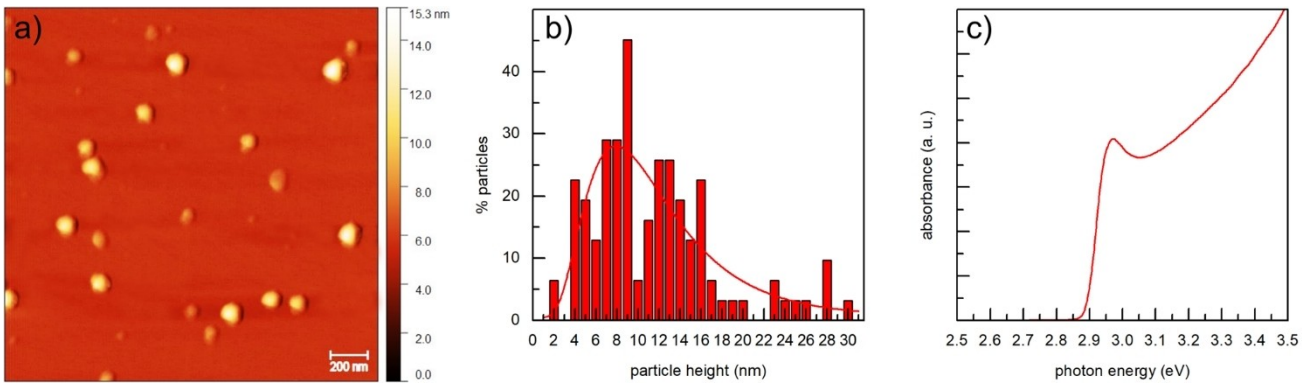

Figure 1. Characterization of AgI NP: a) AFM image of the AgI sample deposited on mica substrate; b) distribution of vertical dimensions of AgI particles and the corresponding fit to log-normal function; c) UV-vis absorption spectrum of the AgI hydrocolloid.

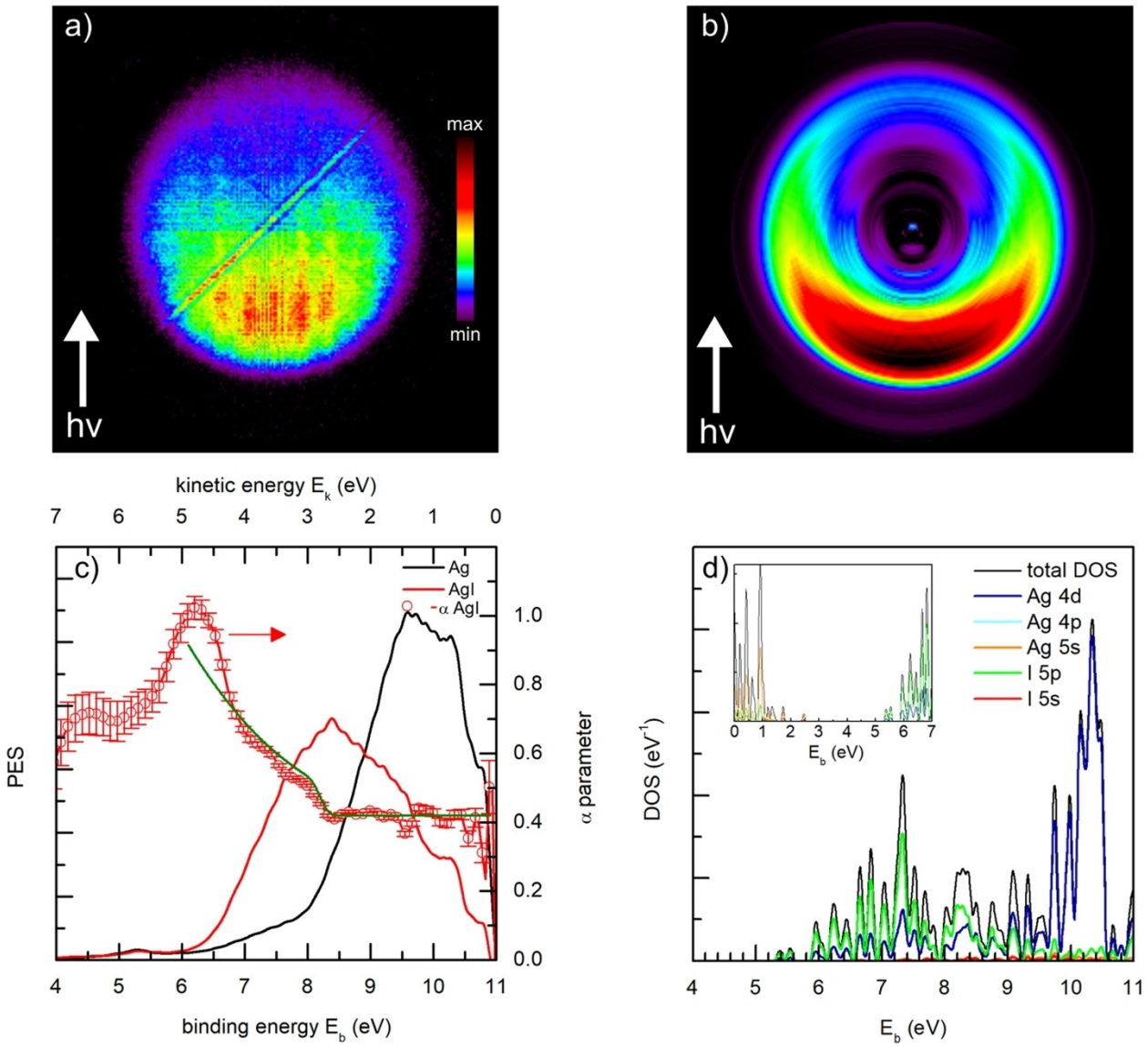

Figure 2. VUV VMI-PES of AgI NP: a) background-corrected and b) α-pBasex reconstructed photoelectron image of isolated AgI NP recorded at hv = 11 eV photon energy. The arrows indicated the direction of the propagation of incident radiation. c) Photoemission spectra of isolated AgI (red lines) and Ag (black line) NP level recorded at hv = 11 eV photon energy. The experimental (red circles) and theoretical (green line) dependence of the asymmetry parameter α on electron energy. d) Total electronic density of states and orbital-projected density of states in the valence region for AgI obtained from DFT/PBE0 calculations. The energy axis corresponds to the zero energy at the vacuum level. The total electronic density of states and the orbital-projected density of states in both valence and the conduction band are given in the inset.

by using circularly polarized radiation and an asymmetric basis set in the inverse Abel transformation, as was shown in our previous study.[29] The electron image for AgI aerosols recorded at hv = 11 eV, reconstructed from the image shown in Figure 2a using the α-pBasex method, is given in Figure 2b. Due to the assumed symmetry around the axis of the propagation of the VUV radiation, the reconstructed image represents a central slice in the three-dimensional distribution of the photoelectron momenta. From the reconstructed image, the photoemission spectrum can be obtained by integrating the electron count over all polar angles for a given distance from the center of the image (which can be directly transformed into electron energy). The extent of the asymmetry in the electron images can be described by the asymmetry parameter α, which is defined as the ratio between the number of electrons emitted in forward and backward directions.[23] The dependence of the asymmetry parameter on electron energy can be calculated from the reconstructed image as the intensity ratio between the forward and backward hemispheres for a given electron energy.[29]

Figure 2c shows the photoemission spectrum of AgI aerosol particles with respect to the vacuum level, recorded at 11 eV photon energy. For comparison, the corresponding spectrum of isolated silver nanoparticles is also presented. Two onsets of photoemission are apparent in the spectrum of AgI aerosols. The first one, which is also present in the spectrum of Ag NP, is at 4.5 ± 0.1 eV binding energy and corresponds to the work

function of silver. The appearance of this onset implies formation of residual silver domains in AgI hydrocolloid as a consequence of the reduction of silver ions to metallic state. The additional threshold is positioned at 6.0 ± 0.1 eV and corresponds to the ionization energy (IE) of AgI. By comparing the experimental IE with the band gap energy from the UV-vis spectrum (Figure 1c), we can estimate the conduction band minimum (CBM) to 3.1 ± 0.2 eV with respect to the vacuum level. To elucidate the contribution of different atomic orbitals to the valence band structure of AgI, we performed DFT/PBE0 calculations. The calculated total electronic density of states and orbital-projected density of states are presented in Figure 2d. Note that the bands obtained from DFT/PBE0 calculations show a valence band maximum at 5.4 eV, followed by an increase in density of states at 6.0 eV, which is in accordance with the valence bands obtained by VUV VMI-PES. The results demonstrate that the valence band of AgI is dominated by the contribution of the Ag 4d and I 5p orbitals, the latter being prevalent in the ionization threshold region. This result is in agreement with our previous study on the valence band structure of Ag–Bi–I nanoplatelets[17] that showed similar ionization energy values due to the major contribution of the I 5p states. The inset to Figure 2d shows that the lowest states in the conduction band originate from the s orbitals of Ag atoms and the s and p orbitals of I atoms. The obtained theoretical band gap was 2.9 eV, which agrees with the experimental UV-Vis result.

The dependence of the α parameter on the electron energy can be directly obtained from the α-pBasex reconstructed electron image (Figure 2b).[29] The $\alpha(E_b)$ dependence for the electron image of AgI aerosols recorded at $h\nu = 11$ eV photon energy is presented in Figure 2c. Note that for the binding energies below the $IE = 6.0 \pm 0.1$ eV, the photoemission from the aerosol particles should be completely symmetric (i.e. $\alpha(E_b) = 1$). However, due to the low signal-to-background ratio in this energy range, the obtained $\alpha(E_b)$ dependence shows nonphysical, more structured, behavior for $E_b < IE$. For that reason, we limit our analyses of the $\alpha(E_b)$ dependence to the [IE, hv] binding energy range. At higher binding energies, the α parameter has a nearly constant value of ~0.42. This value is strongly affected by the absorption length in the aerosol particle and should decrease in the case of homogenous AgI particles of the same size. The asymmetry parameter abruptly increases below $E_b < 8.3$ eV binding energy (above $E_k > 2.7$ eV electron kinetic energy). The observed dependence is typical for the VUV aerosol photoemission, and it is analyzed in detail in our previous study by including the contribution of the inelastically scattered electrons on the α parameter *via* a loss function.[29] In its simplest form, the dependence can be described by[29]

$$\alpha(E_k) \approx \alpha_0 \left(1 + A \times \frac{1}{\mu} E_k \, \Theta(E_k - \omega_c)\right), \quad (1)$$

where $E_k = h\nu - E_b$ is the electron kinetic energy, μ is the effective electron scattering length, α_0~0.42 is the value of the asymmetry parameter at higher binding energies, Θ is the step function, ω_c – is the characteristic electron scattering energy loss, and A is a renormalization constant in units of $eV^{-1}\,nm^{-1}$. Consequently, from the perspective of attenuation only, the asymmetry parameter should vary only smoothly along the valence band and the constant photon energy. However, its rapid increase indicates electron losses due to inelastic scattering processes. The characteristic energy loss in the present system, i.e., the minimal amount of energy that an excited electron loses prior to the photoemission is $\omega_c = 2.7$ eV. The theoretical curve based on Eq. (1), calculated for $\omega_c = 2.7$ eV and assuming universal curve dependence of the electron scattering length on electron energy $\mu \sim E_k^{-2}$, is also presented in Figure 2c. It can be seen that the simplified formula shows good agreement with the experimental curve. For the modeling of the asymmetry parameter dependence at kinetic energies higher than ω_c, a better insight into electron scattering lengths of the material is necessary, as well as the inclusion of the surface scattering by the primary particles.

Also, it is worth noting that the value of the characteristic energy loss is very close to the band gap value. This is in accordance with our previous VUV VMI-PES study on Ag_2S nanoparticles[28] which showed that both the band gap and the ω_c values were ~1 eV. Bearing in mind that the electron energy loss can be related to band-to-band transitions (but also to interstitial excitations or plasmon-related losses), as well as that the leading edge in the loss function of semiconductor nanomaterials is related to exciton formation, this result indicates that the asymmetry parameter dependence on the electron energy can be used to gain additional information on the electronic structure of isolated semiconductor nanoparticles.

Methods

Silver nitrate ($AgNO_3$), sodium borohydride ($NaBH_4$), and potassium iodide (KI) were purchased from Sigma Aldrich and used as received. Mili-Q deionized water with an 18.2 mΩ/cm resistivity was used as a solvent. To prepare AgI NPs, 10 ml of 2 mM $AgNO_3$ aqueous solution was stirred on a magnetic stirrer under an argon atmosphere for ten minutes before quickly adding 1.5 ml of 20 mM KI aqueous solution. The resulting solution was stirred for an additional 10 minutes and appeared clear and bright yellow, indicating the formation of nanoparticles. For comparison to the VUV VMI-PES data, silver nanoparticles were also prepared using the same concentration of silver ions, but instead of KI, $NaBH_4$ was used as a reducing agent.

The UV–Vis absorption spectrum of AgI hydrocolloid was measured using a Shimadzu UV-2600 (Shimadzu Corporation, Japan) spectrophotometer in the 200–800 nm range. The morphology of AgI nanoparticles deposited was recorded by atomic force microscopy (AFM) using a Quesant atomic force microscope. For these analyses, the AgI hydrocolloids were deposited on freshly cleaved mica substrates by spin-coating (3500 rpm, 1 min). AFM microscope was operating in a tapping mode at room temperature, using standard silicon probes Q-

WM300 (force constant 40 N/m). Dimensions and profiles were estimated using Gwyddion software.

The VUV VMI-PES experiments were performed at the variable polarization undulator-based VUV DESIRS beamline of the Synchrotron SOLEIL.[35] The scheme of the experiment on the DESIRS beamline and details of the aerodynamic lens system for focusing aerosol particles are presented in Božanić et al..[29] Briefly, the AgI hydrocolloid was atomized by using a TSI 3076 atomizer, operating under 2.5 bar of argon carrier gas, and passed through a 2 m long diffusion drier filled with silica gel. The obtained aerosol was transported via a 200 μm pinhole into a vacuum chamber equipped with an aerodynamic lens to focus the aerosol particles into a beam. In parallel, the aerosol was characterized by a Scanning Mobility Particle Sizer (SMPS) system (composed of a TSI 3081 differential mobility analyzer with a Kr^{85} neutralizer and a TSI 3772 condensation particle counter). The focused aerosol beam was crossed by 11 eV circularly polarized synchrotron radiation (flux ~10^{12} photons/sec). The photoemitted electrons were discriminated according to their momenta using a 2D position-sensitive detector coupled to a VMI spectrometer. For the 3D reconstruction of photoelectron images, an inverse Abel transformation was performed using the α-pBasex algorithm described previously.[29] The photoemission spectra and the dependence of the asymmetry parameter on the kinetic energy were obtained from the angular and radial integration of the reconstructed images. The photoemission spectra were calibrated relative to the vacuum level using the binding energy of the $3p_{3/2}$ level of argon at 15.76 eV ($^2P_{3/2} \leftarrow {}^1S$).

DFT Calculations

The electronic structure of the wurtzite AgI material and its interface with vacuum was calculated using DFT using a similar approach that we used in our previous work on Ag–Bi–I and BiI_3 materials.[36] First, the lattice parameters and atomic positions of bulk AgI were determined by performing DFT calculations where semilocal Perdew–Burke–Ernzerhof (PBE)[37] exchange-correlation functional was used. Fully relativistic norm-conserving pseudopotentials were used[38,39] and the effects of spin-orbit interaction were included. We obtained the lattice constants of

$a = 4.37$ Å and $c = 7.08$ Å. Second, to obtain the positions of band energies with respect to vacuum, we performed a DFT calculation of the interface of AgI with the vacuum. More precisely, we consider the system consisting of the AgI slab with a width of 4*a* in the nonpolar *a* direction and the vacuum slab of the same width. To obtain the positions of band energies with respect to vacuum, we determined the energy shift that was necessary to align the bulk potential profile with a potential profile in the material slab. When PBE functional was used in the calculations, we obtained the AgI band gap of 1.2 eV and the ionization potential of 4.5 eV. The band gap is underestimated because of the well-known limitation of local and semilocal density functionals. To improve upon these results, we finally performed the calculation of bulk AgI using a hybrid PBE0 functional.[40,41] We use the difference between the VBM levels in PBE0 and PBE bulk calculation to calculate the correction to the VBM. We thus obtain the AgI band gap of 2.9 eV and the ionization potential of 5.4 eV. All calculations were performed using the Quantum Espresso code.[42,43]

Conclusions

We have performed a synchrotron radiation VUV VMI-PES study of isolated aerosol particles (100 nm in size) containing aggregates of 10 nm silver iodide nanoparticles. The aerosols were produced by atomization of the AgI NPs hydrocolloid. The ionization energy of AgI NPs was estimated to be 6.0 ± 0.1 eV with respect to the vacuum level. The photoemission spectrum obtained at a photon energy of 11 eV is rationalized through the calculated orbital-projected density of states for AgI obtained from DFT/PBE0 calculations. The comparison shows that the main contribution to the valence band of AgI is from the I 5p states. The dependence of the asymmetry parameter on the electron energy showed that excited photoelectrons exhibit scattering energy losses with a characteristic value of 2.7 eV, which matches the value of the band gap of the nanomaterial.

It is worth noting that the angular distribution of the photoelectrons, which is represented *via* the dependence of the asymmetry parameter on the electron energy, could provide similar information on the electronic structure of semiconductor nanomaterials as that obtained by low electron energy loss spectroscopy. This is the direct consequence of the attenuation of the VUV radiation in the aerosol particle, which occurs when the absorption length of the incident radiation is smaller than the particle size. On the other hand, the proposed analyses of the angular distribution require non-zero α parameter. Therefore, the analyses would not be efficacious in scenarios involving bulk materials or high-energy photons. However, further studies on different semiconductor nanomaterials and wider electron energy ranges are necessary to provide definite conclusions.

Acknowledgements

The authors acknowledge to Ministry of Science, Technological Development, and Innovation of the Republic of Serbia for financial support (451-03-66/2024-03/200017). The VUV VMI-PES experiments on isolated AgI NPs were performed at the DESIRS beamline at Synchrotron SOLEIL as a part of research project number 20180566. The authors are grateful for the support of the entire staff of Synchrotron SOLEIL for smooth operation during the beamtime. N.V. acknowledges funding provided by the Institute of Physics Belgrade, through a grant from the Ministry of Science, Technological Development, and Innovation of the Republic of Serbia. Numerical computations were performed on the PARADOX-IV supercomputing facility at the Scientific Computing Laboratory, National Center of Excellence for the Study of Complex Systems, Institute of Physics Belgrade.

Conflict of Interests

The authors declare no conflict of interest.

Data Availability Statement

The data that support the findings of this study are available from the corresponding author upon reasonable request.

Keywords: photoelectron spectroscopy · silver iodide nanoparticles · electronic structure · velocity map imaging

[1] N. Ahmad, A. M. Alshehri, Z. R. Khan, I. Ahmad, P. M. Z. Hasan, A. A. Melaibari, M. Shkir, *Mater. Sci. Semicond. Process.* **2022**, *137*, 106239.
[2] Y.-G. Guo, J.-S. Lee, Y.-S. Hu, J. Maier, *J. Electrochem. Soc.* **2007**, *154*, K51.
[3] S. Hull, *Rep. Prog. Phys.* **2004**, *67*, 1233.
[4] C. Tubandt, E. Lorenz, *Zeitschrift für Phys. Chemie* **1914**, *87 U*, 513.
[5] R. Makiura, T. Yonemura, T. Yamada, M. Yamauchi, R. Ikeda, H. Kitagawa, K. Kato, M. Takata, *Nat. Mater.* **2009**, *8*, 476.
[6] S. Yamasaki, T. Yamada, H. Kobayashi, H. Kitagawa, *Chem. Asian J.* **2013**, *8*, 73.
[7] B.-E. Mellander, *Phys. Rev. B* **1982**, *26*, 5886.
[8] T. Yamamoto, M. Maesato, N. Hirao, S. I. Kawaguchi, S. Kawaguchi, Y. Ohishi, Y. Kubota, H. Kobayashi, H. Kitagawa, *J. Am. Chem. Soc.* **2017**, *139*, 1392.
[9] B. Lei, M. Zhu, P. Chen, C. Chen, W. Ma, T. Li, M. Liu, *ACS Appl. Mater. Interfaces* **2014**, *6*, 4160.
[10] Y. Orooji, M. Ghanbari, O. Amiri, M. Salavati-Niasari, *J. Hazard. Mater.* **2020**, *389*.
[11] A. S. Awed, G. S. El-Sayyad, A. El-ghandour, M. F. O. Hameed, M. I. A. Abdel Maksoud, A. I. El-Batal, S. S. A. Obayya, *J. Cluster Sci.* **2019**.
[12] R. A. Ismail, G. M. Sulaiman, M. H. Mohsin, A. H. Saadoon, *IET Nanobiotechnol.* **2018**, *12*, 781.
[13] J. Choi, D. A. Reddy, T. K. Kim, *Ceram. Int.* **2015**, *41*, 13793.
[14] X. Wang, X. Wan, W. Li, X. Chen, *Micro Nano Lett* **2014**, *9*, 376.
[15] M. Khazaee, K. Sardashti, C. C. Chung, J. P. Sun, H. Zhou, E. Bergmann, W. A. Dunlap-Shohl, Q. Han, I. G. Hill, J. L. Jones, D. C. Lupascu, D. B. Mitzi, *J Mater Chem A Mater* **2019**, *7*, 2095.
[16] I. Turkevych, S. Kazaoui, E. Ito, T. Urano, K. Yamada, H. Tomiyasu, H. Yamagishi, M. Kondo, S. Aramaki, *ChemSusChem* **2017**, *10*, 3754.
[17] D. Danilović, A. R. Milosavljević, P. Sapkota, R. Dojčilović, D. Tošić, N. Vukmirović, M. Jocić, V. Djoković, S. Ptasinska, D. K. Božanić, *J. Phys. Chem. C* **2022**, *126*, 13739.
[18] H. C. Sansom, G. Longo, A. D. Wright, L. R. V. Buizza, S. Mahesh, B. Wenger, M. Zanella, M. Abdi-Jalebi, M. J. Pitcher, M. S. Dyer, T. D. Manning, R. H. Friend, L. M. Herz, H. J. Snaith, J. B. Claridge, M. J. Rosseinsky, *J. Am. Chem. Soc.* **2021**, *143*, 3983.
[19] F. Gaie-Levrel, G. A. Garcia, M. Schwell, L. Nahon, *Phys. Chem. Chem. Phys.* **2011**, *13*, 7024.
[20] A. R. Milosavljević, D. K. Božanić, S. Sadhu, N. Vukmirović, R. Dojčilović, P. Sapkota, W. Huang, J. Bozek, C. Nicolas, L. Nahon, S. Ptasinska, *J. Phys. Chem. Lett.* **2018**, *9*, 3604.
[21] L. Ban, B. L. Yoder, R. Signorell, *Annu. Rev. Phys. Chem.* **2020**, *71*, 315.
[22] A. T. J. B. Eppink, D. H. Parker, *Rev. Sci. Instrum.* **1997**, *68*, 3477.
[23] K. R. Wilson, S. Zou, J. Shu, E. Rühl, Stephen, R. Leone, G. C. Schatz, M. Ahmed, *Nano Lett.* **2007**, *7*, 2014.
[24] R. Signorell, M. Goldmann, B. L. Yoder, A. Bodi, E. Chasovskikh, L. Lang, D. Luckhaus, *Chem. Phys. Lett.* **2016**, *658*, 1.
[25] M. I. Jacobs, O. Kostko, M. Ahmed, K. R. Wilson, *Phys. Chem. Chem. Phys.* **2017**, *19*, 13372.
[26] S. Tigrine, N. Carrasco, D. K. Bozanic, G. A. Garcia, L. Nahon, *Astrophys. J.* **2018**, *867*, 164.
[27] F. Süßmann, L. Seiffert, S. Zherebtsov, V. Mondes, J. Stierle, M. Arbeiter, J. Plenge, P. Rupp, C. Peltz, A. Kessel, S. A. Trushin, B. Ahn, D. Kim, C. Graf, E. Rühl, M. F. Kling, T. Fennel, *Nat. Commun.* **2015**, *6*, 7944.
[28] D. Danilović, D. K. Božanić, G. A. Garcia, L. Nahon, U. Stamenović, V. V. Vodnik, V. Djoković, *Opt. Quantum Electron.* **2022**, *54*.
[29] D. K. Božanić, G. A. Garcia, O. Sublemontier, J. Pajović, V. Djoković, L. Nahon, *J. Phys. Chem. C* **2020**, *124*, 24500.
[30] D. K. Božanić, G. A. Garcia, L. Nahon, D. Sredojević, V. Lazić, I. Vukoje, S. P. Ahrenkiel, V. Djoković, Ž. Šljivančanin, J. M. Nedeljković, *J. Phys. Chem. C* **2019**, *123*, 29057.
[31] M. Raşa, B. W. M. Kuipers, A. P. Philipse, *J. Colloid Interface Sci.* **2002**, *250*, 303.
[32] K.-H. Tseng, C.-T. Yeh, M.-Y. Chung, Y.-S. Lin, N. Qui, *Sci. Rep.* **2021**, *11*, 20457.
[33] M. J. Berg, K. R. Wilson, C. M. Sorensen, A. Chakrabarti, M. Ahmed, *J. Quant. Spectrosc. Radiat. Transfer* **2012**, *113*, 259.
[34] M. Goldmann, J. Miguel-Sánchez, A. H. C. West, B. L. Yoder, R. Signorell, *J. Chem. Phys.* **2015**, *142*.
[35] L. Nahon, N. de Oliveira, G. A. Garcia, J.-F. Gil, B. Pilette, O. Marcouillé, B. Lagarde, F. Polack, *J. Synchrotron Radiat.* **2012**, *19*, 508.
[36] D. Danilović, D. K. Božanić, R. Dojčilović, N. Vukmirović, P. Sapkota, I. Vukašinović, V. Djoković, J. Bozek, C. Nicolas, S. Ptasinska, A. R. Milosavljević, *J. Phys. Chem. C* **2020**, *124*, 23930.
[37] J. P. Perdew, K. Burke, M. Ernzerhof, *Phys. Rev. Lett.* **1996**, *77*, 3865.
[38] M. J. van Setten, M. Giantomassi, E. Bousquet, M. J. Verstraete, D. R. Hamann, X. Gonze, G.-M. Rignanese, *Comput. Phys. Commun.* **2018**, *226*, 39.
[39] D. R. Hamann, *Phys. Rev. B* **2013**, *88*, 085117.
[40] J. P. Perdew, M. Ernzerhof, K. Burke, *J. Chem. Phys.* **1996**, *105*, 9982.
[41] C. Adamo, V. Barone, *J. Chem. Phys.* **1999**, *110*, 6158.
[42] P. Giannozzi, O. Andreussi, T. Brumme, O. Bunau, M. Buongiorno Nardelli, M. Calandra, R. Car, C. Cavazzoni, D. Ceresoli, M. Cococcioni, N. Colonna, I. Carnimeo, A. Dal Corso, S. de Gironcoli, P. Delugas, R. A. DiStasio, A. Ferretti, A. Floris, G. Fratesi, G. Fugallo, R. Gebauer, U. Gerstmann, F. Giustino, T. Gorni, J. Jia, M. Kawamura, H.-Y. Ko, A. Kokalj, E. Küçükbenli, M. Lazzeri, M. Marsili, N. Marzari, F. Mauri, N. L. Nguyen, H.-V. Nguyen, A. Otero-de-la-Roza, L. Paulatto, S. Poncé, D. Rocca, R. Sabatini, B. Santra, M. Schlipf, A. P. Seitsonen, A. Smogunov, I. Timrov, T. Thonhauser, P. Umari, N. Vast, X. Wu, S. Baroni, *J. Phys. Condens. Matter* **2017**, *29*, 465901.
[43] P. Giannozzi, S. Baroni, N. Bonini, M. Calandra, R. Car, C. Cavazzoni, D. Ceresoli, G. L. Chiarotti, M. Cococcioni, I. Dabo, A. Dal Corso, S. de Gironcoli, S. Fabris, G. Fratesi, R. Gebauer, U. Gerstmann, C. Gougoussis, A. Kokalj, M. Lazzeri, L. Martin-Samos, N. Marzari, F. Mauri, R. Mazzarello, S. Paolini, A. Pasquarello, L. Paulatto, C. Sbraccia, S. Scandolo, G. Sclauzero, A. P. Seitsonen, A. Smogunov, P. Umari, R. M. Wentzcovitch, *J. Phys. Condens. Matter* **2009**, *21*, 395502.

Manuscript received: March 22, 2024
Revised manuscript received: May 10, 2024
Accepted manuscript online: May 28, 2024
Version of record online: July 18, 2024

ChemPhysChem

Supporting Information

Velocity Map Imaging Photoelectron Spectroscopy of Silver Iodide Aerosol Particles

Danijela Danilović,* Laurent Nahon, Gustavo A. Garcia, Aleksandar R. Milosavljević, Nenad Vukmirović, Radovan Dojčilović, Dragana Tošić, Vladimir Djoković, and Dušan K. Božanić*

Supporting Information

Velocity Map Imaging Photoelectron Spectroscopy of Silver Iodide Aerosol Particles

Danijela Danilović*, Laurent Nahon, Gustavo A. Garcia, Aleksandar R. Milosavljević, Nenad Vukmirović, Radovan Dojčilović, Dragana Tošić, Vladimir Djoković, and Dušan K. Božanić*

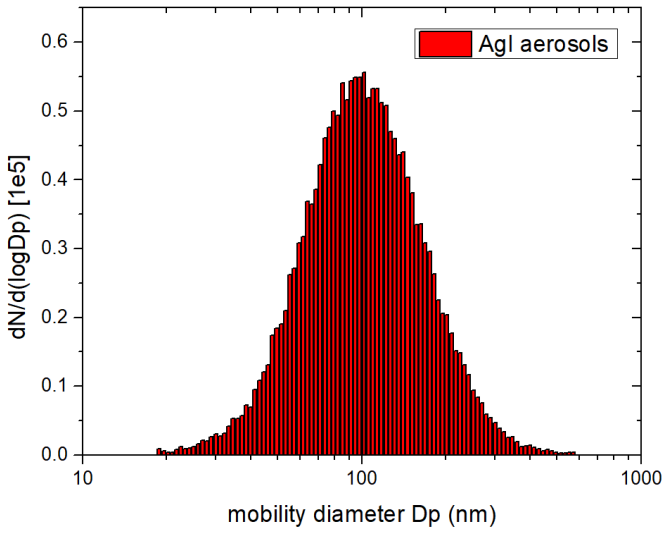

Figure S1. Distribution of mobility diameters of AgI aerosol particles measured by the SMPS.